

Original citation:

Liu, Jun, Hao, X. J., Zhou, L., Strangwood, M., Davis, C. L. and Peyton, A. J.. (2012) Measurement of microstructure changes in 9Cr–1Mo and 2.25Cr–1Mo steels using an electromagnetic sensor. *Scripta Materialia*, Volume 66 (Number 6). pp. 367-370. ISSN 1359-6462

Permanent WRAP url:

<http://wrap.warwick.ac.uk/67570>

Copyright and reuse:

The Warwick Research Archive Portal (WRAP) makes this work by researchers of the University of Warwick available open access under the following conditions. Copyright © and all moral rights to the version of the paper presented here belong to the individual author(s) and/or other copyright owners. To the extent reasonable and practicable the material made available in WRAP has been checked for eligibility before being made available.

Copies of full items can be used for personal research or study, educational, or not-for profit purposes without prior permission or charge. Provided that the authors, title and full bibliographic details are credited, a hyperlink and/or URL is given for the original metadata page and the content is not changed in any way.

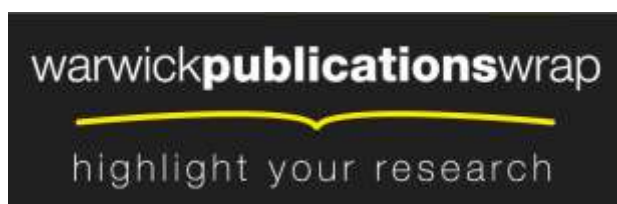
Publisher's statement:

© 2012, Elsevier. Licensed under the Creative Commons Attribution-NonCommercial-NoDerivatives 4.0 International <http://creativecommons.org/licenses/by-nc-nd/4.0/>

A note on versions:

The version presented here may differ from the published version or, version of record, if you wish to cite this item you are advised to consult the publisher's version. Please see the 'permanent WRAP url' above for details on accessing the published version and note that access may require a subscription.

For more information, please contact the WRAP Team at: publications@warwick.ac.uk



<http://wrap.warwick.ac.uk>

Measurement of microstructure changes in 9Cr-1Mo and 2.25Cr-1Mo steels using an electromagnetic sensor

J. Liu^{a,1}, X.J. Hao^a, L. Zhou^a, M. Strangwood^a, C.L. Davis^a, A.J. Peyton^b

^a School of Metallurgy & Materials, University of Birmingham, Edgbaston, Birmingham B15 2TT, UK

^b School of Electrical and Electronic Engineering, University of Manchester, Manchester M60 1QD, UK

Abstract

This paper presents results from a multi-frequency electromagnetic sensor used to characterise the microstructural changes in 9Cr-1Mo and 2.25Cr-1Mo power generation steels after tempering and elevated temperature service exposure. The electromagnetic sensor can detect the microstructural changes in both steels due to the corresponding relative permeability and resistivity changes. The low frequency inductance value is particularly sensitive to the different relative permeability values of both steels.

Keywords: EM sensor, relative permeability, electrical resistivity, power plant steels

Microstructural changes during operation of elevated temperature power generation steels alter their properties and their remaining safe operating life (remnant life) [1]. Efficient operation of power generation plant requires the microstructural condition to be assessed during service. Currently the microstructural state is assessed using replicas of the surface or inferred from hardness measurements, both taken during shut down

¹ Corresponding author: sam.j.liu@gmail.com; j.liu.7@bham.ac.uk;

periods. Non-destructive evaluation (NDE) of microstructural changes in power plant steels during their service life is of interest to aid in the determination of safe remnant life. Amongst a wide range of NDE techniques available, electromagnetic (EM) methods are of particular interest in evaluation of ferromagnetic ferritic heat resistant steels. EM sensors can be used in a non-contact fashion (with stand-off distances of over 10 mm) and can survey through (non-magnetic non-conducting) coatings. Ferritic Cr-Mo alloy steels are commonly used for heavy section power plant components such as steam line pipes, boiler tubes and turbine rotors operating at temperatures from around 560 °C to 630 °C. Future operating temperatures may increase to 650 °C in order to increase the thermal efficiency of power plant [2].

Cr-Mo-based creep-resisting steels, such as the 2.25 Cr-1 Mo, 9 Cr and 12 Cr families, are normalised, quenched and tempered, or normalised and tempered at service entry with their microstructures consisting of a tempered lath martensite (lath widths about 0.3-0.5 μm) strengthened by alloy carbides [3]. During elevated temperature service (usually for 10s of years) the microstructure evolves gradually by [3]:

1. Coarsening of the fine tempered martensite laths into broader ferrite laths.
2. Coarsening of the fine M_2X carbides into larger, more equilibrium M_{23}C_6 and/or M_6C carbides.
3. Finally the formation of an equiaxed ferrite grain structure with grain growth and the concentration of coarser carbides on ferrite grain boundaries.

Multi-frequency EM sensors have proved sensitive to the change of ferrite/austenite fraction [4, 5], shown using model alloys, in-situ analysis and modelling, and decarburisation [6, 7], shown for high carbon steels for on-line and off-line monitoring. Proto-type EM sensors are being used for in-situ monitoring of steel processing [8]. The theory as to how the relative permeability and resistivity of a sample affects the multi-frequency EM response is presented elsewhere [9]. It has been reported that the microstructural changes in power plant steels e.g. 9Cr-1Mo[10, 11], 2.25Cr-1Mo[10] subjected to long tempering and 5Cr-0.5Mo [12] subjected to creep testing result in changes to their magnetic properties. Therefore multi-frequency EM sensors should be able to detect the relative permeability (dominant effect) and resistivity (minor effect) changes, resulting from microstructural changes in power plant steels during service at high temperatures. To assess the sensitivity of a multi-frequency EM sensor to changes in microstructure, this paper has studied the EM sensor response to P9 and T22 power generation steel samples representative of initial service entry and long-term exposure microstructures.

The P9 and T22 steels studied were removed from a refinery furnace at a petrochemical plant after approximately 11 years at 520 °C (comparable with equivalent elevated temperature service at a power generation plant [13]). Their chemical compositions are given in Table 1. Selected samples (approx. 70mm×15mm×7mm) were heat treated to simulate the service entry microstructure, i.e. tempered martensite / bainite, by normalising at 950°C for 1 hour or 940 °C for 1 hour followed by air cooling to room temperature and then tempering at 760°C for 1 hour or 720 °C for 1.5 hours for

P9 and T22 respectively. As-normalised samples were also examined. The heat treatment conditions have been determined as per ASTM standards A335 [14] and A213 [15] as well as literature data [10, 16-19].

Metallographic samples were polished to 0.25 μ m and etched in Kallings for P9 and 2% nital for T22. Scanning electron microscope (SEM) micrographs were obtained using a JEOL-6060. A four-point probe technique was employed to independently measure the resistivity of the steels with a direct current Cropico DO5000 microhmmeter at room temperature using cylinder specimens of 4.95 mm in diameter and 50.0 mm in length. The resistivity values used as input into the Comsol model (described later) to predict the relative permeability values.

A cylindrical EM sensor, similar to that used in [6], consisting of one exciting coil and one sensing coil both wound around an insulating tube of 5.5 mm and 6.5 mm inner and outer diameters respectively was used. EM sensor tests were carried out on the same cylindrical specimens as for the resistivity measurements. The sensor was operated at 3V and a range of frequencies from 10 Hz to 1 MHz. Signals picked up by the sensing coil were recorded and processed by an Impedance Analyzer (Model S1260) made by Solartron Analytical measuring complex trans-impedance Z , from which mutual inductance L was calculated by $L = Z/j \omega$, where ω is angular frequency and j the imaginary unit.

The microstructure of the as-normalised P9 consists of predominantly martensite mixed with some bainite as shown in Fig. 1(a). Subsequent tempering produces a

simulated service entry microstructure, i.e. tempered martensite / bainite as shown in Fig. 1(b). After long service exposure, the microstructure showed equiaxed ferrite with large carbides distributed within ferrite grains or on grain boundaries as shown in Fig. 1(c).

The electrical resistivity measurements of all the samples are given in Table 2. The tempering heat treatment has resulted in a 7.49% resistivity drop compared to the as-normalised P9 value. In contrast, the ex-service resistivity decrease compared with the normalised and tempered value is only 0.46% despite the large microstructural changes as described above. This is due to the resistivity value being most affected by the change in dislocation density and elements (for example carbon) in solution between the as-normalised condition and tempered condition, with the service exposure resulting in little further change in these factors.

Fig. 2 (a) show the EM sensor measurements of the P9 samples as the real part of mutual inductance as a function of frequency. The real inductance is essentially independent of frequency over the low frequency (approx 10 - 100 Hz) range then drops continuously with increasing frequency until it approaches a near zero value at very high frequencies (over approximately 0.1 MHz). For conciseness the inductance value at low frequencies (here taken as the mean value for the first 5 data points from 10 to 25 Hz) has been used as a characteristic parameter L_0 ; the values of which are given in Table 2.

The L_0 of the as-tempered P9 is 45% lower than that of the service exposed value and 37.5% higher than the as-normalised value. Over the low frequency range, the

relative permeability dominates the L_0 value as the eddy currents are insignificant. As the frequency increases eddy currents strengthen (and the effect of resistivity strengthens accordingly) and reduce the mutual inductance, which accounts for the decreasing (damping) part of real inductance as shown in Fig. 2 (a).

A 2D axisymmetric finite element (FE) model was developed for modelling the sensor signal output in response to a steel sample of given resistivity and relative permeability using Comsol Multiphysics. The model is broadly similar to that described in [6]. The resistivity values of modelled samples were taken from the experimental measurements and the relative permeability values determined by fitting the modelled real inductance with the experimental measurement based on a non-linear least square method with 51 frequency points from 10 Hz to 1MHz in Comsol LiveLink for Matlab. It should be noted that fitting was also carried out for both the relative permeability and resistivity (to account for a situation where this value was unknown, e.g. during inspection of power plant components) and the difference in values obtained was very small (e.g. only 0.55% for the as-tempered and 1.65% for the service exposed P9). Close fits between the modelled and measured real inductance for all the samples have been achieved as shown in Fig. 2. The fitted relative permeability values are presented in Table 2 as well as plotted as a function of low frequency inductance values in Fig. 3. Fig. 3 indicates that the relative permeability values exponentially increase with corresponding low frequency inductance for both P9 and T22 steels in the different heat treated conditions.

During the service exposure for P9, when the resistivity change is negligible, the significant increase (>100%) in relative permeability can be attributed to the annihilation of the ferrite lath boundaries (formed of dislocation networks in tempered martensite) reducing the number of pinning points affecting domain wall motion. Carbide coarsening, that mainly takes place on prior austenite grain boundaries, however, is expected not to significantly affect the domain wall pinning or contribute much to change in relative permeability because these carbides are so widely separated and some of them are, by this stage, so coarse (typically $1\text{-}2\mu\text{m} \times 0.5\text{-}1\mu\text{m}$) that their interfaces with the matrix becoming semi-coherent or incoherent can act as sites for reverse domains to be nucleated [20]. On nucleation, the domain walls will make larger movements because both there is increased energy stored and the pinning from these particles will be released [21]. The resistivity drop during tempering, which is slightly greater than during the service exposure, has a negligible influence on the low frequency inductance value according to Comsol modelling of the real inductance with a fixed relative permeability and changing resistivity values. Therefore, the increase in relative permeability during tempering for P9 can be ascribed to the change in microstructural features including a considerable decrease in the dislocation density in the strained martensite laths of the as-normalized P9, and as a result of changes in the laths to a larger lath size, as can be seen in Fig. 1(a) and (b). These factors are expected to have a more dominant effect than the precipitation of carbides occurring mostly on lath and prior austenite grain boundaries, which play a relatively minor role in pinning domain

walls as the grain/lath boundaries appear to be the major pinning points in this case [22, 23].

The as-normalised T22 steel shows a mixed microstructure of bainite and some proeutectoid ferrite as shown in Fig. 4(a). No carbides are present in the ferrite, but plate-like carbides can be seen within the bainite region. After tempering many carbides can be observed along prior austenite grain boundaries, on ferrite boundaries or within bainite regions as shown in Fig. 4(b). The microstructure of T22 after the service exposure consists of equiaxed ferrite and a great many carbides outlining the ferrite grain boundaries or finely dispersed within the ferrite grains as shown in Fig. 4(c).

Compared to P9 the T22 steel samples have much lower resistivity values due to a much lower content of solute alloy elements. However, the resistivity decrease due to service exposure and tempering are more significant than in P9, being 9.00% and 17.79% respectively.

The EM sensor measurements of the T22 samples in terms of the real part of mutual inductance as a function of frequency, is shown in Fig. 2 (b). The L_0 of the T22 changes on tempering and after service exposure in a similar manner as the P9 although to a lesser extent. There has been an 11.2% increase of L_0 after service and 13.1% after tempering, corresponding to a 14.7% and 23.0% increase in relative permeability after service and tempering respectively.

There should be very low mobile dislocation densities present in both the T22 and P9 samples after a long service exposure. In comparison with P9, the service exposed T22

has a much lower relative permeability although it has, on average, a larger ferrite grain size, which would be expected to permit more domain wall motion before encountering a grain boundary and hence a higher relative permeability. However the service exposed T22 contains more carbide precipitates, which appears to be providing more pinning points for domain wall motion. This may be due to their fine dispersion within the grains giving rise to a shorter mean free path for domain wall motion. This outweighs the difference in ferrite grain size and accounts for the lower relative permeability value.

The as-tempered T22 has a slightly higher relative permeability value compared with the as-tempered P9, which can be attributed to a slightly larger lath size in T22 and a similar distribution of carbides, that is, mainly on lath and prior austenite grain boundaries as well as being comparable in number as can be observed in Fig. 1(b) and Fig. 3(b). For the normalised condition, the higher relative permeability value for the T22 is as expected from the higher proportion of bainite consisting of ferrite laths with carbides present (and proeutectoid ferrite, which is known to have a higher permeability [6, 7]) rather than the strained martensite laths with a high dislocation density present in the as-normalised P9.

In conclusion, the present multi-frequency EM sensor has proved sensitive to relatively small microstructural changes in both P9 and T22 steels during tempering and service that can be related to the changes in their resistivity and relative permeability. The real inductance at low frequencies L_0 is particularly affected by differences in the relative permeability of the steels studied, which is found to increase exponentially with the L_0 values in the range studied.

This work was carried out with financial support from EPSRC under the grant EP/H023429/1.

- [1] B. Raj, V. Moorthy, T. Jayakumar, K.B.S. Rao, *INT MATER REV*, 48 (2003) 273-325.
- [2] F. Masuyama, *ISIJ INT*, 41 (2001) 612-625.
- [3] P. Ennis, A. Czyska-Filemonowicz, *SADHANA-ACAD P ENG S*, 28 (2003) 709-730.
- [4] W. Yin, X.J. Hao, A.J. Peyton, M. Strangwood, C.L. Davis, *NDT & E INT*, 42 (2009) 64-68.
- [5] S.J. Dickinson, R. Binns, W. Yin, C. Davis, A.J. Peyton, *IEEE T INSTRUM MEAS*, 56 (2007) 879-886.
- [6] X. Hao, W. Yin, M. Strangwood, A. Peyton, P. Morris, C. Davis, *METALL MATER TRANS A*, 40 (2009) 745-756.
- [7] X.J. Hao, W. Yin, M. Strangwood, A.J. Peyton, P.F. Morris, C.L. Davis, *SCRIPTA MATER*, 58 (2008) 1033-1036.
- [8] A.J. Peyton, W. Yin, S.J. Dickinson, C.L. Davis, M. Strangwood, X. Hao, A.J. Douglas, P.F. Morris, *IRONMAK STEELMAK*, 37 (2010) 135-139.
- [9] R.J. Haldane, W. Yin, M. Strangwood, A.J. Peyton, C.L. Davis, *SCRIPTA MATER*, 54 (2006) 1761-1765.
- [10] V. Moorthy, S. Vaidyanathan, B. Raj, T. Jayakumar, B. Kashyap, *METALL MATER TRANS A*, 31 (2000) 1053-1065.
- [11] A. Mitra, J.N. Mohapatra, J. Swaminathan, M. Ghosh, A.K. Panda, R.N. Ghosh, *SCRIPTA MATER*, 57 (2007) 813-816.

- [12] J.N. Mohapatra, N.R. Bandyopadhyay, M.K. Gunjan, A. Mitra, J MAGN MAGN MATER, 322 (2010) 589-595.
- [13] H.C. Furtado, L.H. de Almeida, I. Le May, MATER CHARACT, 58 (2007) 72-77.
- [14] ASTM standards A335/A335M -09a, 2009
- [15] ASTM standards A213/A213M - 09b, 2009
- [16] S. Saroja, M. Vijayalakshmi, V.S. Raghunathan, MATER T JIM, 34 (1993) 901-906.
- [17] B. Arivazhagan, R. Prabhu, S. Albert, M. Kamaraj, S. Sundaresan, J MATER ENG PERFORM, 18 (2009) 999-1004.
- [18] J.R. Yang, C.Y. Huang, C.N. Yang, J.L. Horng, MATER CHARACT, 30 (1993) 75-88.
- [19] G. Sangdahl, M. Semchyshen, Application of 2¼Cr-1 Mo Steel for Thick-Wall Pressure Vessels, ASTM 1982.
- [20] I.n. Lin, R. Mishra, G. Thomas, IEEE T MAGN, 20 (1984) 134-139.
- [21] D.J. Buttle, J.P. Jakubovics, G.A.D. Briggs, C.B. Scruby, PHILOS MAG A, 55 (1987) 735-756.
- [22] A.D. Beale, J.P. Jakubovics, M.G. Hetherington, C.B. Scruby, B.A. Lewis, K.J. Davies, J MAGN MAGN MATER, 104-107 (1992) 365-367.
- [23] J.A. Baldwin Jr, P.W. Smith Jr, F. Milstein, SOLID STATE COMMUN, 17 (1975) 973-974.

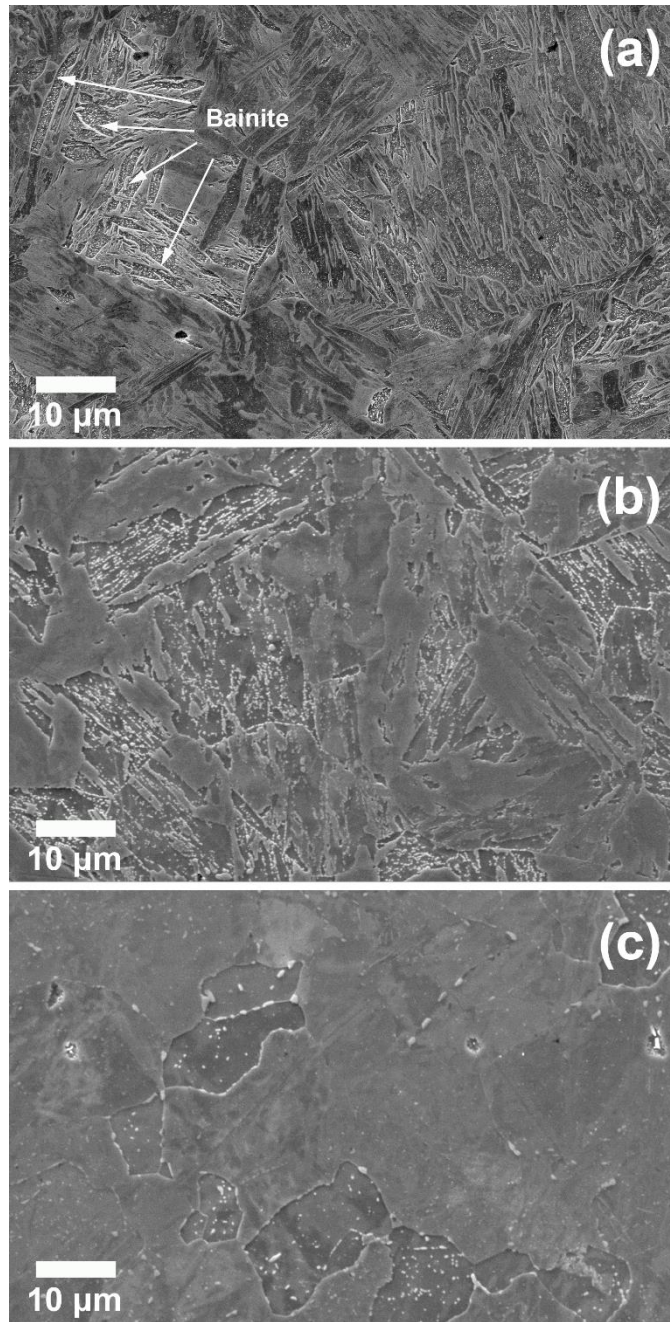


Fig. 1 Microstructure of the P9 samples in the different heat treated conditions. (a) as normalized, (b) normalized and tempered and (c) ex-service.

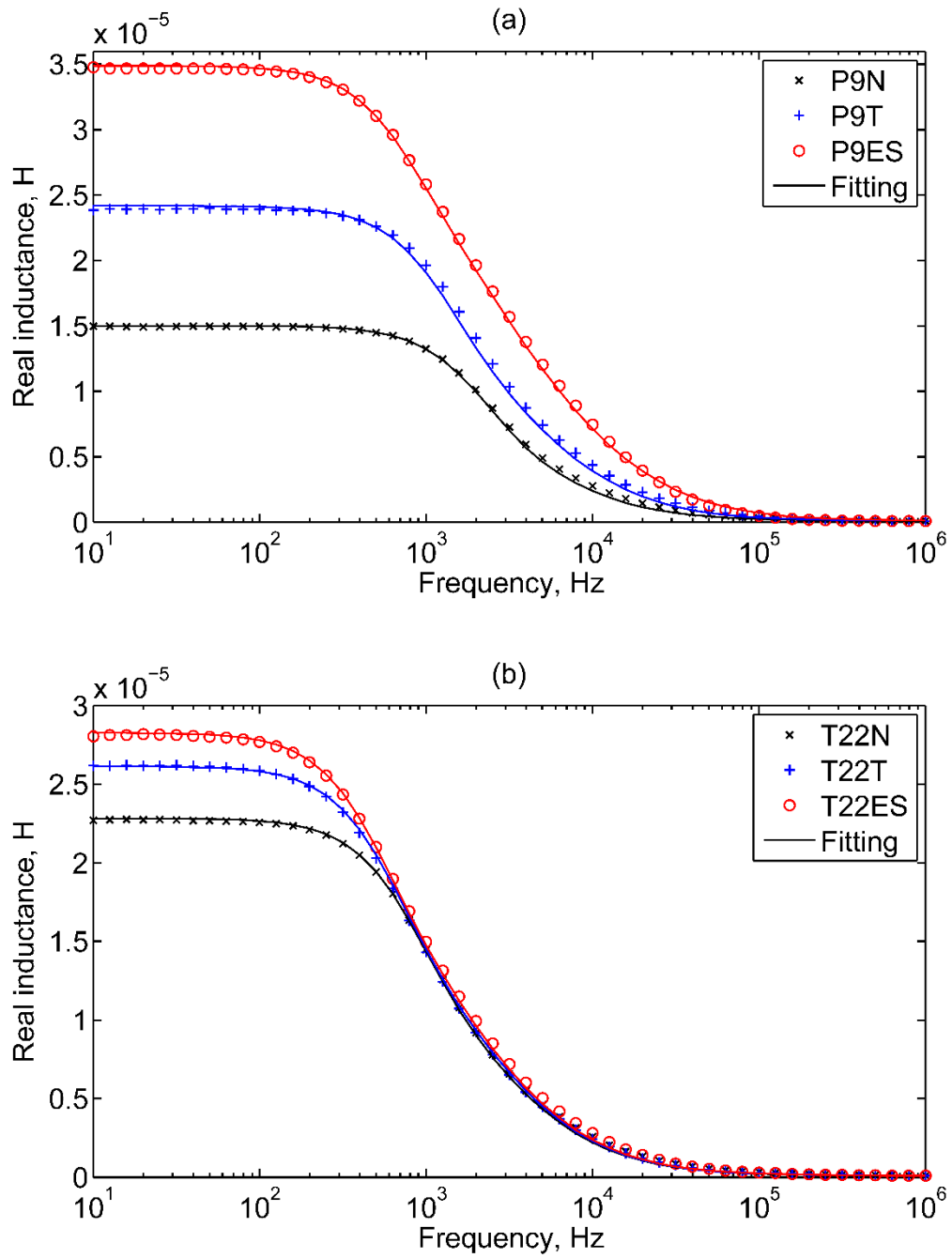


Fig. 2 Real mutual inductance of EM sensor coils as a function of frequency for (a) P9 and (b) T22.

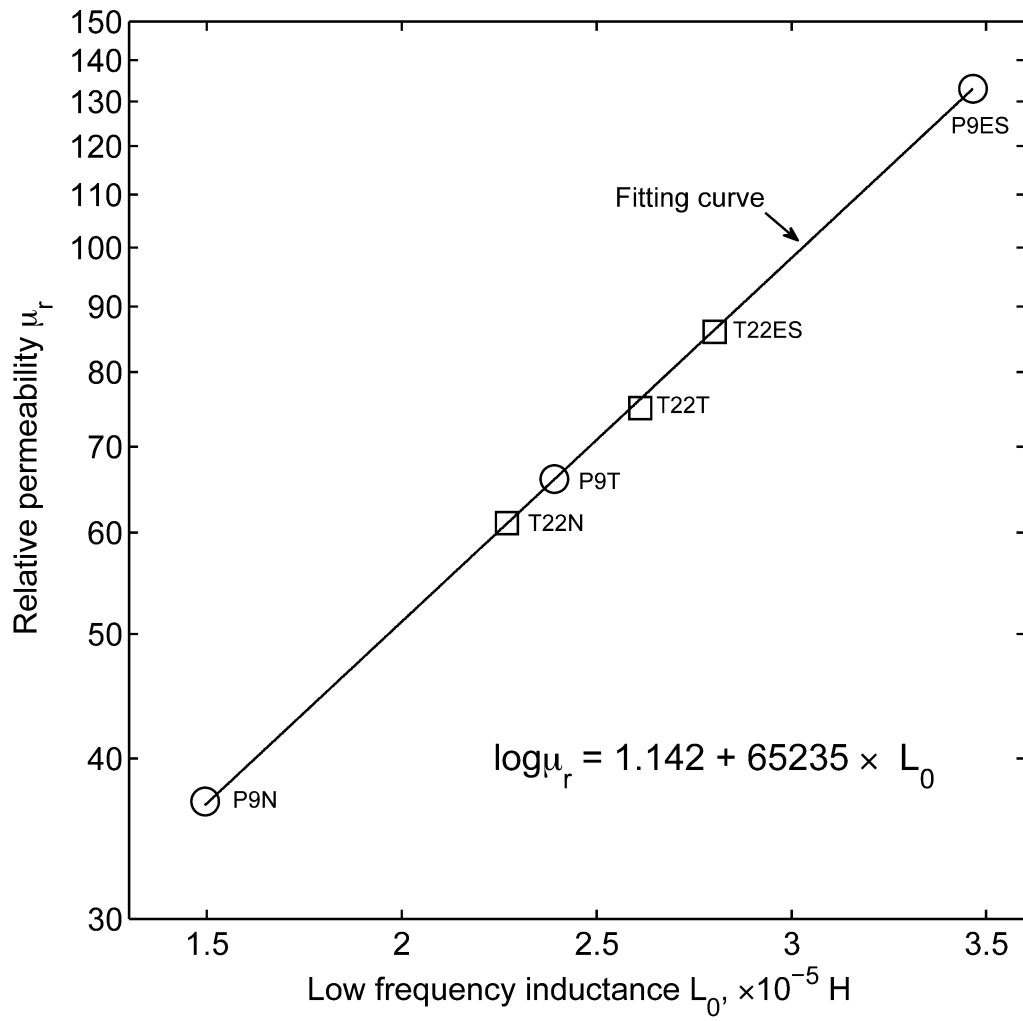


Fig. 3 Relative permeability as a function of low frequency inductance for both P9 and T22 samples in the different heat treated conditions fitting well with an exponential relationship.

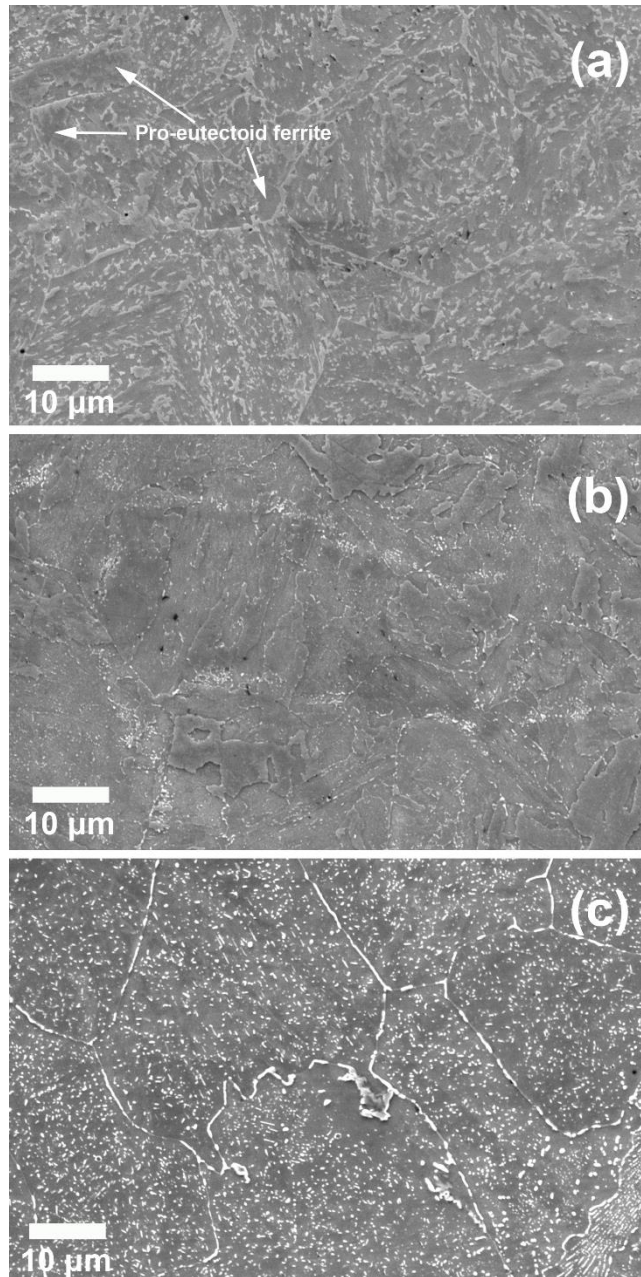


Fig. 4 Microstructure of the T22 samples in the different heat treated conditions. (a) as normalized, (b) normalized and tempered and (c) ex-service